Fission barriers and saddle shapes in nuclei of A∼200

K. Mahata*
Nuclear Physics Division, Bhabha Atomic Research Centre, Mumbai - 400085, INDIA

Fission fragment angular distributions have been measured for ^{12,13}C+^{192,194,196,198}Pt systems in the laboratory energy range from 60 to 80 MeV. Statistical model calculations (for compound nucleus decay) in conjunction with Statistical Saddle Point Model (SSPM) (for fission fragment anisotropy) calculations were carried out to explain the observed anisotropy. Statistical model analysis of the fission excitation function and prefission neutron multiplicity data indicates the persistence of shell correction to the liquid drop energy at the saddle point for all systems studed. SSPM calculation of fission fragment angular anisotropy using Rotating Finite Range Model (RFRM) effective moment of inertia ($\Im_{\rm eff}$) differ from the measured data. Good agreement could be obtained by normalising RFRM $\Im_{\rm eff}$ values with energy independent factor. A correlation between weighted average ground state quadrupole moments and extracted $\Im_{\rm eff}$ values have been observed. Present results imply that microscopic corrections to liquid drop surface are significant even at large deformation (saddle point) and at high temperature ($< T >\sim 1$ MeV at the saddle point) in this mass region.

1. Introduction

In fission a single nucleus splits into two fragments of roughly equal mass. This drastic rearrangements process exhibits both statistical and dynamical features and is governed by the delicate interplay between the macroscopic aspects of bulk nuclear matter and the quantal effects of a finite number of nucleons. Determination of the height of the barrier (B_f) and the position of the saddle point remained as key issues in fission since its discovery [1]. Fission barrier height is a important ingredient in understanding the heavy-ion induced fusion-fission reactions and in prediction of super heavy elements. Accurate knowledge of fission barrier heights is also required for the study of stellar nucleosynthesis and energy applications [2]. The importance of the position of the saddle point in controlling the dynamics of heavy ion induced fusion-fission reaction has been beautifully illustrated by Möller and Sierk [3].

Remarkable progress has been made in the calculation of potential energy surface to understand various observations in fission [1]. It is well established that the fission barriers of actinide nuclei have double-humped shapes due to the influence of nuclear shell effects around the saddle point shapes. In nuclei of A∼ 200, shell corrections are not expected to lead to any significant minimum in the nuclear deformation potential energy because of much steeper variation in the liquid drop energy with deformation. However, a significant shell correction may be present at the saddle point deformation of these nuclei, as indicated by some calculations [4–6]. Experimental information regarding shell correction energy at the saddle point deformation for A∼200 is scarce. Measurement of fission fragment mass, in Coulomb excited fission [7] and fusion fission [8], showed symmetric distributions implying absence of significant shell corrections at the saddle point deformation in this mass region. Recent unexpected discovery of asymmetric fission of ^{180}Hg following electron capture decay of ^{180}Tl [9] has generated intense interest in this field.

In case of actinide nuclei, fission barriers are smaller and can be directly measured experimentally. However, most of the measurements of fission cross sections for A ∼200 are performed at energies much higher than that of fission barrier, where there are other competing channels open and statistical description become essential. In the statistical model for the decay of compound nucleus, the competition between fission and light particle emission is determined by the relative density of levels

*Electronic address: kmahata@barc.gov.in

available. The density of levels depends upon available excitation energy (U_x) and level density parameter (a_x). Here, $x = n$ or f corresponding to equilibrium or saddle point deformation.

Although a number of studies have been carried out, there are still ambiguities in choosing various input parameters for the statistical model analysis. In earlier attempts to extract fission barrier heights from the fits to the measured fission excitation functions, excitation functions of evaporation residues (ER) and prefission neutron multiplicities (ν_{pre}) were not considered. It has been shown that the fission cross sections, which are cumulative, can be explained by several sets of correlated pairs of fission barrier (B_f) and ratio of level density parameter ($\tilde{a}_f/\tilde{a}_n$) [10]. However, simultaneous fits to the excitation functions of fission, evaporation residue and prefission neutron multiplicities can be obtained by unique set of parameters. In this talk, recent results of fission fragment angular distribution measurement in nuclei of A$\sim$200 will be presented.

2. Measurement Details

The fission fragment angular distributions for ^{12,13}C+^{192,194,196,198}Pt system have been measured using the BARC-TIFR 14 UD Pelletron accelerator at Mumbai. The measurements have been carried out in the laboratory energy range from 60 to 80 MeV, using self-supporting rolled foils of ^{192}Pt (^{192}Pt 57.0%, ^{194}Pt 26.2%, ^{195}Pt 11.2%, ^{196}Pt 4.7%, 1.0 mg/cm^2 thick), ^{194}Pt (97.4% enriched, 0.98 mg/cm^2 thick), ^{196}Pt (96.2% enriched, 1.7 mg/cm^2 thick) and ^{198}Pt (95.7% enriched, 1.4 mg/cm^2 thick). Fission fragment angular distributions were measured from 80° to 170° in laboratory using ΔE-E telescopes consisting of Si surface barrier detectors (thicknesses ΔE 10-22 μm, E 300 μm). Most of the fission fragments were stopped in ΔE detector while fragments reaching the E detector were well separated from the direct reaction products and evaporated particles in the two dimensional ΔE vs E plot. Two Si surface barrier detectors, kept at 30° and 40° to monitor

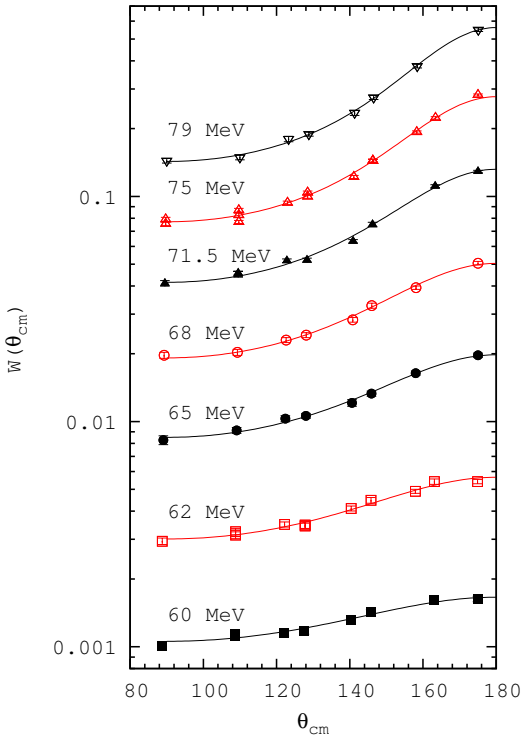

FIG. 1: Measured fission fragment angular distributions for ^{12}C+^{192}Pt as a function of centre-of-mass angle. Lines are fits to the data using the standard expression for angular distribution (see text).

Rutherford scattering, were used for absolute normalization of fission cross sections.

Measured fission fragment angular distributions were transformed to centre-of-mass making use of kinematic variables estimated from Violas systematics [12] for symmetric fission. Angular distributions in center of mass ($W(\theta)$) were fitted with the standard expression for angular distribution [13, 14]. Measured angular distributions for ^{12}C+^{192}Pt system along with the fit is shown in Fig. 1. Total fission cross-sections (σ_{fiss}) were obtained by integrating the measured angular distributions. The fission excitation functions are shown in Fig 2. Fission excitation functions for a given target with ^{12}C and ^{13}C are

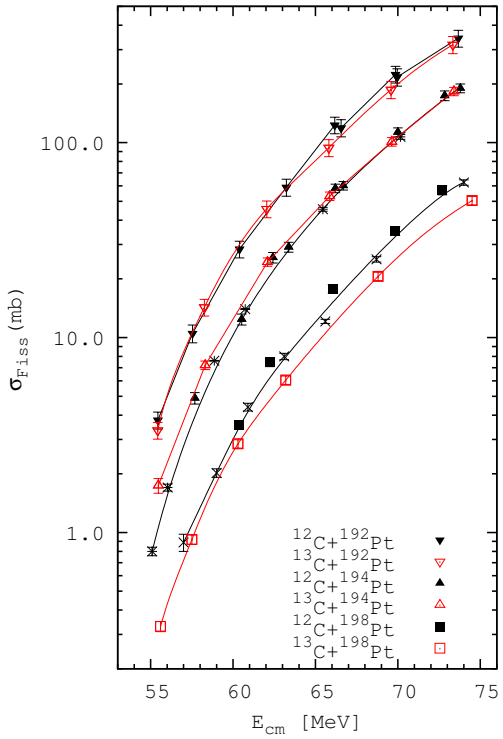

FIG. 2: Measured fission excitation functions for ^{12,13}C+$^{192,194,198}Pt$ systems. The asterisks and crosses represents fission cross sections for ^{12}C+^{194,198}Pt from Ref. [11], respectively. Lines are to guide the eye.

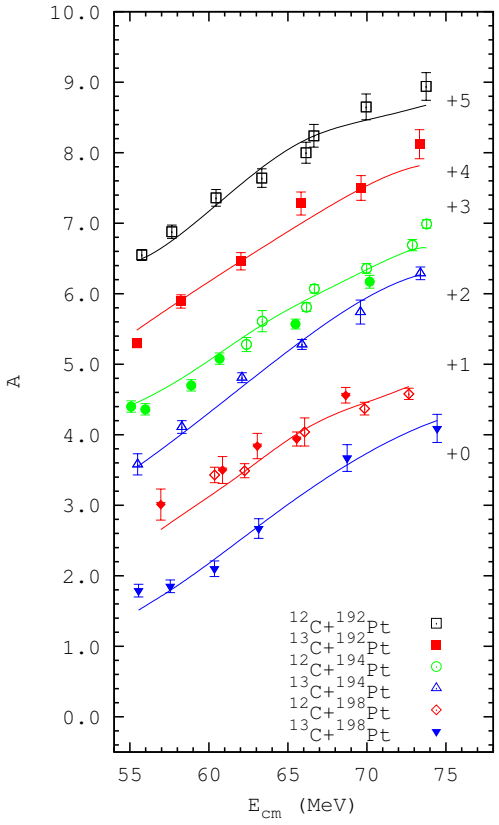

FIG. 3: (Color online) Experimental fission fragment angular anisotropy (A) values for ^{12,13}C+^{192,194,198}Pt systems. The filled circles and filled diamonds represents the data for ^{12}C+^{194,198}Pt from Ref. [11], respectively.The the continuous lines are the SSPM calculations.

found to be similar. Fission fragment angular anisotropies (A), defined as $W(180°)/W(90°)$, are shown in Fig 3.

3. Statistical model analysis

Statistical model analysis of the measured fission probabilities (ratio of fission to fusion cross sections) were carried out using the code PACE [15] with a shell corrected fission barrier and level density prescription [10]. Fusion cross excitation functions for ^{12}C+^{194,198}Pt systems are taken from Ref. [16]. Initial compound nucleus spin (J) distributions have been generated using CCFULL [17] after fitting the fusion excitation functions. Measured fusion excitation functions for both ^{12}C+^{194}Pt system and ^{12}C+^{198}Pt system are found to be similar. Hance, the fusion cross sections for fusion ^{12}C+^{192,196}Pt systems are assumed to be same. In case of systems with ^{13}C projectile, same nuclear potential have been use to calculate fusion cross sections and initial spin distributions.

In the analysis, fission barrier is expressed as $B_f(J) = B_{LD}(J) - \Delta_n + \Delta_f$, where $B_{LD}(J)$, Δ_n and Δ_f are the J dependent liquid drop component of the fission barrier, the shell correction at the ground state and the shell correction at the saddle point, respectively. The values of $B_{LD}(J)$ are taken from

rotating finite range model [18]. The shell correction at the ground state is taken as the difference between the experimental and liquid drop mass. The shell correction at the saddle point is assumed to be $k_f \times \Delta_n$. An energy dependent shell correction to the level density parameter $a_x = \tilde{a_x}[1 + (\Delta_x/U_x)(1 - e^{-\eta U_x})]$ is employed with $x = n$ or f corresponding to equilibrium or saddle deformation. The asymptotic liquid drop values $\tilde{a_n}$ and $\tilde{a_f}$ are taken to be $A/9$ and $\tilde{a_f}/\tilde{a_n} \times \tilde{a_n}$, respectively.

The values of k_f and $\tilde{a_f}/\tilde{a_n}$ are varied to fit the fission probabilities (P_f) and prefission neutron multiplicities (ν_{pre}) simulteneously. Prefission neutron multiplicities are taken from systematics [19]. Measured fission probabilities along with the statistical model fits are shown in Fig. 4. Corresponding fission barrier heights are shown in Fig. 5. As can be seen from Fig. 4, the increase in fission probability is smaller while going from odd mass number to even mass compound nuclei as compared to those while going from even mass number to odd mass compound nuclei. Same feature is also observed in Fig. 5. even mass compound nuclei show higher fission barriers as compared to those for adjacent odd mass compound nuclei. As observed in our earlier analysis [10], a significant fraction of the ground state shell correction persists at the saddle point for the present systems. It should be noted here that the extracted fission barrier heights from the present analysis are significantly lower than those extracted earlier analysis [20] of fission excitation function assuming only first chance fission (ν_{pre}=0).

4. Statistical Saddle Point Model (SSPM) analysis

In order to calculate fission fragment angular distributions, the angular momentum distributions and the temperature appropriate for each fissioning nucleus have to be estimated. Statistical model discussed above have been used to estimate the distributions of the fissioning nuclei in E^* and J after fitting the fission probabilities and ν_{pre} values. Fission fragment angular anisotropy values are calculated according to SSPM [21] using the

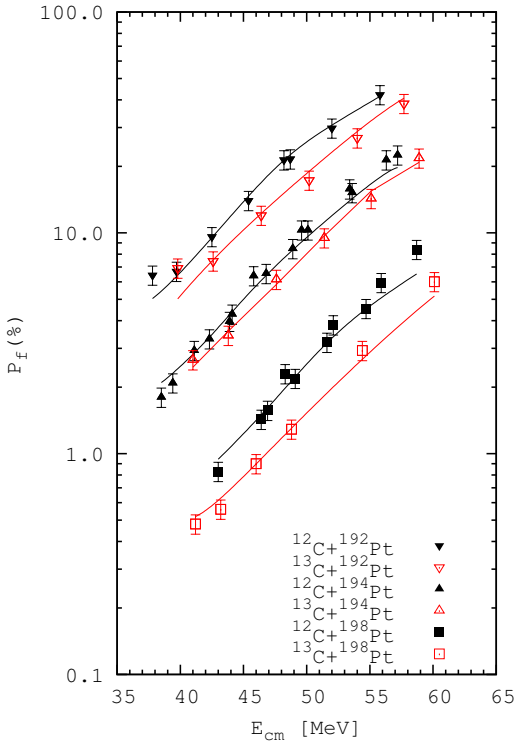

FIG. 4: Measured fission probabilities are compared with the statistical model calculations (continuous lines) for ^{12,13}C+^{192,194,198}Pt systems.

(E^*, J) distributions of the fissioning nuclei for each chance. The exact expression for angular distribution has been used to calculate fission fragment anisotropy values as discussed in Ref [22]. Anisotropy values calculated using values of $\Im_{eff}$ from RFRM [18] are found to differ from the data. Hence, the $\Im_{eff}$ values from RFRM were normalized with E^* and J independent factors to fit the measured fission anisotropy data. Calculated anisotropy values are compared with the experimental data in Fig. 3. Good agreement could be obtained for all the systems by normalising the RFRM $\Im_{eff}$ values with E^* and J independent factor.

Fig. 6 (a) and (b) show the weighted average ground state shell corrections (Δ_n^{WA}) and weighted average ground state quadrupole de-

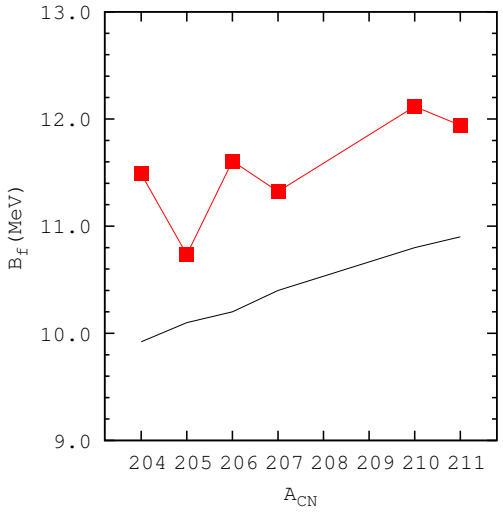

FIG. 5: Fission barrier heights (filled squares) corresponding to the best fits to the fission probabilities and prefission neutron multiplicities. The continuous line is the RFRM prediction.

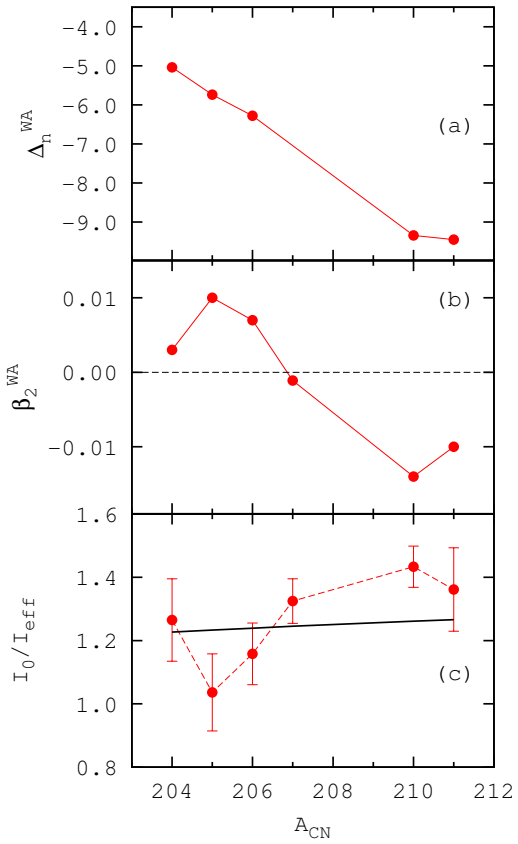

FIG. 6: Weighted average value of ground state (a) shell corrections and (b) quadrupole deformation of the fissioning nuclei. (c) The ratio of the moment of inertia of rigid sphere to the effective moment of inertia at the saddle point ($\Im_0/\Im_{eff}$) required to fit the experimental anisotropy data. The continuous line is the RFRM prediction.

formation (β_2^{WA}), respectively. Weighted averaging has been done over the fissioning nuclei at E_{cm} = 65 MeV. The values of β_2 have been taken from Ref. [23]. In Fig. 6 (c) the ratio of the moment of inertia of rigid sphere to the effective moment of inertia at the saddle point ($\Im_0/\Im_{eff}$) required to fit the experimental anisotropy data are compared with the RFRM predictions (continuous line). Value of $\Im_0/\Im_{eff}$ smaller (larger) than RFRM predictions less (more) compact saddle shape as compared to RFRM prediction. While the value of $-\Delta_n^{WA}$ increases monotonously as mass number increases, a correlation between β_2^{WA} and $\Im_0/\Im_{eff}$ has been observed. As β_2^{WA} goes from +ve (prolate) to −ve (oblate), $\Im_0/\Im_{eff}$ goes from smaller to larger than RFRM prediction (more compact to less compact saddle shape as compared to RFRM prediction).

5. Summary

Fission fragment angular distributions have been measured for ^{12,13}C+^{192,194,196,198}Pt systems at laboratory energy range from 60 MeV to 80 MeV. Statistical model (for compound nucleus decay) and Statistical Saddle Point Model (for fission fragment anisotropy) calculation have been carried out to explain the fission angular anisotropy data. Statistical model analysis of the fission excitation function and prefission neutron multiplicity data indicate that a significant fraction of the ground state shell correction persists at the saddle point for the present systems as observed for other systems in this mass region [10].

Fission fragment anisotropy calculated using RFRM $\Im_{eff}$ values found to differ from the measured data. Good agreement between the SSPM calculations and measured data could be obtained by normalising the RFRM $\Im_{eff}$ values with E^* and J independent factors. A correlation between weighted average ground state quadrupole moments and extracted effective moment of inertia at the saddle point has been observed. It should be noted here that the required values of $\Im_{eff}$ to fit the anisotropy data are sensitive to the input fusion J distributions. However, the relative differences of $\Im_{eff}$ for different systems remain same if the same procedure is followed for all the systems. Present result imply that microscopic corrections to liquid drop surface are important even at large deformation (saddle point) and at high temperature ($< T > \sim$ 1 MeV at the saddle point) in this mass region. These results will provide constraint to the models used to predict stability for super heavy elements.

Acknowledgments

This work was done in collaboration with A. Shrivastava, S.K. Pandit, K. Ramachandran, C. Palshetkar, A. Kumar, P. Patle, A. Parihari, S. Santra, A. Chatterjee and S. Kailas. .

References

[1] P. Möller, A. J. Sierk, T. Ichikawa, A. Iwamoto, R. Bengtsson, H. Uhrenholt, and S. Åberg, Phys. Rev. C **79**, 064304 (2009).

[2] International Atomic Energy Agency, *Handbook for calculation of nuclear reaction data: Reference input parameter library, RIPL-2*, Vienna (2004), URL `http://ndswebserver.iaea.org/RIPL2/`.

[3] P. Möller and A. J. Sierk, Nature **422**, 485 (2003).

[4] H. C. Pauli, T. Ledergerber, and M. Brack, Phys. Lett. **B 34**, 264 (1971).

[5] U. Mosel and H. W. Schmitt, Phys. Rev. **C 4**, 2185 (1971).

[6] M. Bolsterli, O. E. Fiset, J. R. Nix, and J. L. Norton, Phys. Rev. **C 5**, 1050 (1972).

[7] K.-H. Schmidt, J. Benlliure, and A. Junghans, Nuclear Physics A **693**, 169 (2001).

[8] M. G. Itkis, S. M. Luk'yanov, V. N. Okolovich, Y. E. Penionzhkevich, A. Y. Rusanoy, V. S. Salamatin, G. N. Smirenkin, and G. G. Chubarian, Yad. Fiz. **52**, 23 (1990).

[9] A. N. Andreyev, J. Elseviers, M. Huyse, P. Van Duppen, S. Antalic, A. Barzakh, N. Bree, T. E. Cocolios, V. F. Comas, J. Diriken, et al., Phys. Rev. Lett. **105**, 252502 (2010).

[10] K. Mahata, S. Kailas, and S. Kapoor, Phys. Rev. **C 74**, 041301(R) (2006).

[11] A. Shrivastava, S. Kailas, A. Chatterjee, A. M. Samant, A. Navin, P. Singh, and B. S. Tomar, Phys. Rev. Lett. **82**, 699 (1999).

[12] V. Viola, K. Kwiatkowski, and M. Walker, Phys. Rev. **C 31**, 1550 (1985).

[13] K. Mahata, S. Kailas, A. Shrivastava, A. Chatterjee, P. Singh, and S. Santra, Phys. Rev. **C 65**, 034613 (2002).

[14] B. B. Back, Phys. Rev. **C 31**, 2104 (1985).

[15] A. Gavron, Phys. Rev. **C 21**, 230 (1980).

[16] A. Shrivastava, S. Kailas, A. Chatterjee, A. Navin, A. M. Samant, P. Singh, S. Santra, K. Mahata, B. S. Tomar, and G. Pollarolo, Phys. Rev. **C 63**, 054602 (2001).

[17] K. Hagino, N. Rowley, and A. Kruppa, Comput. Phys. Comm. **123**, 143 (1999).

[18] A. J. Sierk, Phys. Rev. **C 33**, 2039 (1986).

[19] H. Baba, A. Shinohara, T. Saito, N. Takahashi, and A. Yokoyama, Jour. of the Phys. Soci. of Japan **66**, 998 (1997).

[20] L. G. Moretto, K. X. Jing, R. Gatti, G. J. Wozniak, and R. P. Schmitt, Phys. Rev. Lett. **75**, 4186 (1995).

[21] R. Vandenbosch and J. R. Huizenga, *Nuclear Fission* (Academic Press, NewYork, 1973).

[22] K. Mahata, S. Kailas, A. Shrivastava, A. Chatterjee, A. Navin, P. Singh, S. Santra, and B. Tomar, Nucl. Phys. **A720**, 209 (2003).

[23] P. Möller, J. R. Nix, W. D. Myers, and W. J. Swiatecki, Atomic Data Nuclear Data Tables **59**, 185 (1995).